Biomedical Optics EXPRESS

Quantifying collagen structure in breast biopsies using second-harmonic generation imaging

Raghu Ambekar,[1,2] Tung-Yuen Lau,[1,3] Michael Walsh,[4] Rohit Bhargava,[5] and Kimani C. Toussaint, Jr.[1,3,6,*]

[1]*Photonics Research of Bio/nano Environments (PROBE), Department of Mechanical Science and Engineering, University of Illinois Urbana-Champaign, 1206 W Green St, Urbana, IL 61801, USA*
[2]*Department of Electrical and Computer Engineering, University of Illinois Urbana-Champaign, 1406 W Green St, Urbana, IL 61801, USA*
[3]*Department of Mechanical Science and Engineering, University of Illinois Urbana-Champaign, 1206 W Green St, Urbana, IL 61801, USA*
[4]*Beckman Institute for Advanced Science and Technology, University of Illinois Urbana-Champaign, 405 North Mathews Avenue, Urbana, IL 61801, USA*
[5]*Department of Bioengineering, University of Illinois Urbana-Champaign, 1304 W Springfield Avenue, Urbana, IL 61801, USA*
[6]*Affiliate in the departments of Electrical and Computer Engineering, and Bioengineering, University of Illinois Urbana-Champaign, Urbana, IL 61801, USA*
**ktoussai@illinois.edu*

Abstract: Quantitative second-harmonic generation imaging is employed to assess stromal collagen in normal, hyperplastic, dysplastic, and malignant breast tissues. The cellular scale organization is quantified using Fourier transform-second harmonic generation imaging (FT-SHG), while the molecular scale organization is quantified using polarization-resolved second-harmonic generation measurements (P-SHG). In the case of FT-SHG, we apply a parameter that quantifies the regularity in collagen fiber orientation and find that malignant tissue contains locally aligned fibers compared to other tissue conditions. Alternatively, using P-SHG we calculate the ratio of tensor elements (d_{15}/d_{31}, d_{22}/d_{31}, and d_{33}/d_{31}) of the second-order susceptibility χ^2 for collagen fibers in breast biopsies. In particular, d_{15}/d_{31} shows potential differences across the tissue pathology. We also find that trigonal symmetry (*3m*) is a more appropriate model to describe collagen fibers in malignant tissues as opposed to the conventionally used hexagonal symmetry (*C6*). This novel method of targeting collagen fibers using a combination of two quantitative SHG techniques, FT-SHG and P-SHG, holds promise for breast tissue analysis and applications to characterizing cancer in a manner that is compatible with clinical practice.

OCIS codes: (180.4315) Nonlinear microscopy; (100.2960) Image analysis.

References and links

1. A. Jemal, F. Bray, M. M. Center, J. Ferlay, E. Ward, and D. Forman, "Global cancer statistics," CA Cancer J. Clin. **61**(2), 69–90 (2011).
2. "Cancer Facts & Figures—2012," (American Cancer Society, 2012).
3. B. N. Datta, *Textbook of Pathology* (Jaypee Brothers Medical, 2008).
4. S. Srivastava, *Molecular Pathology of Early Cancer* (IOS, 1998).
5. L. A. Liotta, C. N. Rao, and S. H. Barsky, "Tumor invasion and the extracellular matrix," Lab. Invest. **49**(6), 636–649 (1983).
6. D. Radisky, J. Muschler, and M. J. Bissell, "Order and disorder: the role of extracellular matrix in epithelial cancer," Cancer Invest. **20**(1), 139–153 (2002).
7. J. E. Ferguson, A. M. Schor, A. Howell, and M. W. J. Ferguson, "Changes in the extracellular matrix of the normal human breast during the menstrual cycle," Cell Tissue Res. **268**(1), 167–177 (1992).
8. I. Stamenkovic, "Extracellular matrix remodelling: the role of matrix metalloproteinases," J. Pathol. **200**(4), 448–464 (2003).

#168709 - $15.00 USD Received 21 May 2012; revised 19 Jul 2012; accepted 4 Aug 2012; published 7 Aug 2012

9. O. W. Petersen, H. L. Nielsen, T. Gudjonsson, R. Villadsen, F. Rank, E. Niebuhr, M. J. Bissell, and L. Rønnov-Jessen, "Epithelial to mesenchymal transition in human breast cancer can provide a nonmalignant stroma," Am. J. Pathol. **162**(2), 391–402 (2003).
10. S. E. Holton, M. J. Walsh, A. Kajdacsy-Balla, and R. Bhargava, "Label-free characterization of cancer-activated fibroblasts using infrared spectroscopic imaging," Biophys. J. **101**(6), 1513–1521 (2011).
11. S. E. Holton, M. J. Walsh, and R. Bhargava, "Subcellular localization of early biochemical transformations in cancer-activated fibroblasts using infrared spectroscopic imaging," Analyst (Lond.) **136**(14), 2953–2958 (2011).
12. J. T. Erler and V. M. Weaver, "Three-dimensional context regulation of metastasis," Clin. Exp. Metastasis **26**(1), 35–49 (2009).
13. J. Helleman, M. P. Jansen, K. Ruigrok-Ritstier, I. L. van Staveren, M. P. Look, M. E. Meijer-van Gelder, A. M. Sieuwerts, J. G. M. Klijn, S. Sleijfer, J. A. Foekens, and E. M. Berns, "Association of an extracellular matrix gene cluster with breast cancer prognosis and endocrine therapy response," Clin. Cancer Res. **14**(17), 5555–5564 (2008).
14. D. Barkan, J. E. Green, and A. F. Chambers, "Extracellular matrix: a gatekeeper in the transition from dormancy to metastatic growth," Eur. J. Cancer **46**(7), 1181–1188 (2010).
15. P. P. Provenzano, K. W. Eliceiri, J. M. Campbell, D. R. Inman, J. G. White, and P. J. Keely, "Collagen reorganization at the tumor-stromal interface facilitates local invasion," BMC Med. **4**(1), 38 (2006).
16. P. P. Provenzano, D. R. Inman, K. W. Eliceiri, J. G. Knittel, L. Yan, C. T. Rueden, J. G. White, and P. J. Keely, "Collagen density promotes mammary tumor initiation and progression," BMC Med. **6**(1), 11 (2008).
17. C. Thrasivoulou, G. Virich, T. Krenacs, I. Korom, and D. L. Becker, "Optical delineation of human malignant melanoma using second harmonic imaging of collagen," Biomed. Opt. Express **2**(5), 1282–1295 (2011).
18. W. R. Zipfel, R. M. Williams, R. Christie, A. Y. Nikitin, B. T. Hyman, and W. W. Webb, "Live tissue intrinsic emission microscopy using multiphoton-excited native fluorescence and second harmonic generation," Proc. Natl. Acad. Sci. U.S.A. **100**(12), 7075–7080 (2003).
19. P. J. Campagnola and L. M. Loew, "Second-harmonic imaging microscopy for visualizing biomolecular arrays in cells, tissues and organisms," Nat. Biotechnol. **21**(11), 1356–1360 (2003).
20. A. Zoumi, A. Yeh, and B. J. Tromberg, "Imaging cells and extracellular matrix in vivo by using second-harmonic generation and two-photon excited fluorescence," Proc. Natl. Acad. Sci. U.S.A. **99**(17), 11014–11019 (2002).
21. I. Freund, M. Deutsch, and A. Sprecher, "Connective tissue polarity. Optical second-harmonic microscopy, crossed-beam summation, and small-angle scattering in rat-tail tendon," Biophys. J. **50**(4), 693–712 (1986).
22. G. Cox, E. Kable, A. Jones, I. K. Fraser, F. Manconi, and M. D. Gorrell, "3-dimensional imaging of collagen using second harmonic generation," J. Struct. Biol. **141**(1), 53–62 (2003).
23. W. L. Chen, T. H. Li, P. J. Su, C. K. Chou, P. T. Fwu, S. J. Lin, D. Kim, P. T. C. So, and C. Y. Dong, "Second harmonic generation chi tensor microscopy for tissue imaging," Appl. Phys. Lett. **94**, 3 (2009).
24. F. Tiaho, G. Recher, and D. Rouède, "Estimation of helical angles of myosin and collagen by second harmonic generation imaging microscopy," Opt. Express **15**(19), 12286–12295 (2007).
25. R. M. Williams, W. R. Zipfel, and W. W. Webb, "Interpreting second-harmonic generation images of collagen I fibrils," Biophys. J. **88**(2), 1377–1386 (2005).
26. R. Ambekar, M. Chittenden, I. Jasiuk, and K. C. Toussaint, Jr., "Quantitative second-harmonic generation microscopy for imaging porcine cortical bone: comparison to SEM and its potential to investigate age-related changes," Bone **50**(3), 643–650 (2012).
27. R. A. Rao, M. R. Mehta, S. Leithem, and K. C. Toussaint, Jr., "Quantitative analysis of forward and backward second-harmonic images of collagen fibers using Fourier transform second-harmonic-generation microscopy," Opt. Lett. **34**(24), 3779–3781 (2009).
28. R. A. Rao, M. R. Mehta, and K. C. Toussaint, Jr., "Fourier transform-second-harmonic generation imaging of biological tissues," Opt. Express **17**(17), 14534–14542 (2009).
29. M. Sivaguru, S. Durgam, R. Ambekar, D. Luedtke, G. Fried, A. Stewart, and K. C. Toussaint, Jr., "Quantitative analysis of collagen fiber organization in injured tendons using Fourier transform-second harmonic generation imaging," Opt. Express **18**(24), 24983–24993 (2010).
30. P. J. Su, W. L. Chen, J. B. Hong, T. H. Li, R. J. Wu, C. K. Chou, S. J. Chen, C. Hu, S. J. Lin, and C. Y. Dong, "Discrimination of collagen in normal and pathological skin dermis through second-order susceptibility microscopy," Opt. Express **17**(13), 11161–11171 (2009).
31. C. Odin, T. Guilbert, A. Alkilani, O. P. Boryskina, V. Fleury, and Y. Le Grand, "Collagen and myosin characterization by orientation field second harmonic microscopy," Opt. Express **16**(20), 16151–16165 (2008).
32. S. Psilodimitrakopoulos, D. Artigas, G. Soria, I. Amat-Roldan, A. M. Planas, and P. Loza-Alvarez, "Quantitative discrimination between endogenous SHG sources in mammalian tissue, based on their polarization response," Opt. Express **17**(12), 10168–10176 (2009).
33. S. Psilodimitrakopoulos, S. I. C. O. Santos, I. Amat-Roldan, A. K. N. Thayil, D. Artigas, and P. Loza-Alvarez, "In vivo, pixel-resolution mapping of thick filaments' orientation in nonfibrilar muscle using polarization-sensitive second harmonic generation microscopy," J. Biomed. Opt. **14**(1), 014001–014011 (2009).
34. P. J. Su, W. L. Chen, T. H. Li, C. K. Chou, T. H. Chen, Y. Y. Ho, C. H. Huang, S. J. Chang, Y. Y. Huang, H. S. Lee, and C. Y. Dong, "The discrimination of type I and type II collagen and the label-free imaging of engineered cartilage tissue," Biomaterials **31**(36), 9415–9421 (2010).
35. X. Han, R. M. Burke, M. L. Zettel, P. Tang, and E. B. Brown, "Second harmonic properties of tumor collagen: determining the structural relationship between reactive stroma and healthy stroma," Opt. Express **16**(3), 1846–1859 (2008).

#168709 - $15.00 USD Received 21 May 2012; revised 19 Jul 2012; accepted 4 Aug 2012; published 7 Aug 2012

36. T. Hompland, A. Erikson, M. Lindgren, T. Lindmo, and C. de Lange Davies, "Second-harmonic generation in collagen as a potential cancer diagnostic parameter," J. Biomed. Opt. **13**(5), 054050 (2008).
37. B. E. A. Saleh and M. C. Teich, *Fundamentals of Photonics* (Wiley Interscience, 2007).
38. P. N. Butcher and D. Cotter, *The Elements of Nonlinear Optics* (Cambridge University Press, 2003).
39. B. Y. Jiang and S. W. Chu, "Trigonal symmetry of type I collagen probed by SHG polarization anisotropy," in *Conference on Lasers and Electro-Optics/Quantum Electronics and Laser Science Conference and Photonic Applications Systems Technologies*, OSA Technical Digest (CD) (Optical Society of America, 2008), paper JWA30.
40. J. T. Kwak, R. Reddy, S. Sinha, and R. Bhargava, "Analysis of variance in spectroscopic imaging data from human tissues," Anal. Chem. **84**(2), 1063–1069 (2012).
41. I. W. Levin and R. Bhargava, "Fourier transform infrared vibrational spectroscopic imaging: integrating microscopy and molecular recognition," in *Annual Review of Physical Chemistry* (Annual Reviews, Palo Alto, 2005), Vol. 56, pp. 429–474.
42. D. C. Fernandez, R. Bhargava, S. M. Hewitt, and I. W. Levin, "Infrared spectroscopic imaging for histopathologic recognition," Nat. Biotechnol. **23**(4), 469–474 (2005).
43. S. Brasselet, D. Aït-Belkacem, A. Gasecka, F. Munhoz, S. Brustlein, and S. Brasselet, "Influence of birefringence on polarization resolved nonlinear microscopy and collagen SHG structural imaging," Opt. Express **18**(14), 14859–14870 (2010).
44. I. Gusachenko, G. Latour, and M. C. Schanne-Klein, "Polarization-resolved Second Harmonic microscopy in anisotropic thick tissues," Opt. Express **18**(18), 19339–19352 (2010).
45. O. De Wever and M. Mareel, "Role of tissue stroma in cancer cell invasion," J. Pathol. **200**(4), 429–447 (2003).
46. E. Makareeva, S. J. Han, J. C. Vera, D. L. Sackett, K. Holmbeck, C. L. Phillips, R. Visse, H. Nagase, and S. Leikin, "Carcinomas contain a matrix metalloproteinase-resistant isoform of type I collagen exerting selective support to invasion," Cancer Res. **70**(11), 4366–4374 (2010).
47. S. J. Han, E. Makareeva, N. V. Kuznetsova, A. M. DeRidder, M. B. Sutter, W. Losert, C. L. Phillips, R. Visse, H. Nagase, and S. Leikin, "Molecular mechanism of type I collagen homotrimer resistance to mammalian collagenases," J. Biol. Chem. **285**(29), 22276–22281 (2010).
48. M. Hidalgo and S. G. Eckhardt, "Development of matrix metalloproteinase inhibitors in cancer therapy," J. Natl. Cancer Inst. **93**(3), 178–193 (2001).

1. Introduction

Breast cancer is both a leading cause of cancer deaths and among the most frequently diagnosed cancers in women worldwide [1]. In 2012, it is estimated that ~227,000 new patients will be newly diagnosed and ~40,000 will die from breast cancer in the US alone [2]. In humans, almost all breast cancers arise from an uncontrolled growth of aberrant epithelial cells that originate either in the milk ducts or lobules and are categorized as ductal or lobular carcinoma, respectively. Excessive growth within human tissues can result in dense cellular masses ranging from hyperplasia to malignant tumors [3,4]. Though there are more cells in hyperplastic tissue, cellular structure and tissue morphology is similar to normal tissue. In dysplasia, both the cells and their organization are abnormal while neoplasia can be benign, potentially malignant (pre-cancer), or malignant (cancer). Most diagnostic and mechanistic studies in breast cancers focus on epithelial cells and significantly less work has been reported on the role of surrounding stroma and its extracellular matrix (ECM). Stromal involvement and its use as a diagnostic tool, however, is a rapidly emerging concept and is of keen contemporary interest [5–9]. A number of molecular and imaging techniques have been used to characterize the stroma [10–13]. In particular, the ECM predominantly contains type I fibrillar collagen [14], which has been recognized as being important for the initiation and progression of breast cancer [15–17]. Despite these promising results, the lack of analytical techniques to image the ECM is a major barrier to quantifying stromal role in breast cancer progression and, potentially, to a diagnostic protocol.

A useful tool for investigating collagen fiber organization is second-harmonic generation (SHG) imaging, which has recently gained popularity for imaging collagen fibers in biological tissues [18–20]. SHG is a second-order, nonlinear optical process which originates from structures possessing non-centrosymmetry (i.e., those with no center of inversion symmetry) and a high second-order nonlinear coefficient, such as collagen fibers [21,22]. That is, when intense incident light interacts with the collagen fibers, it generates light at twice the incident frequency or half the incident wavelength. Since SHG is emitted mainly from collagen fibers, high-contrast images of collagen-based tissues can be obtained when used in an imaging modality. Moreover, since the intensity of the emitted second-harmonic

#168709 - $15.00 USD Received 21 May 2012; revised 19 Jul 2012; accepted 4 Aug 2012; published 7 Aug 2012

signal varies as the square of the incident light intensity, the excitation can be confined to a sub-femtoliter focal volume, thereby making it feasible to obtain 3D images.

There has been much recent effort in developing useful metrics for quantifying collagen fiber organization utilizing SHG microscopy [23–25]. Quantification facilitates extraction of sensitive changes in collagen fiber organization due to damage or disease, and, thus, may help in early diagnosis. Studies are needed, however, that establish this approach as a clinically-compatible technique with a specific protocol for diagnostic use. Hence, the potential of SHG to understand and provide diagnostic information as well as technology development for this use are needed. As a first step towards that goal, here we first investigate the relative effectiveness of two techniques, Fourier transform-second harmonic generation imaging (FT-SHG) and polarization-resolved second-harmonic generation (P-SHG). FT-SHG involves utilizing 2D spatial Fourier transforms of SHG images to quantify collagen fiber organization at cellular scales (300 nm–100 μm) [26–29]. Metrics such as preferred fiber orientation have previously been used to successfully assess tendon injury as well as to explore age-related structural changes in cortical bone [26,29]. P-SHG exploits the coherent signal generation by modulating the incident light polarization to obtain normalized tensor elements of the second-order susceptibility coefficient (χ^2) of collagen fibers [21,23,24,30–33]. Assuming that type I collagen fibers possess cylindrical symmetry (*C6*) crystal class, it has previously been shown that χ^2 can be used to differentiate between type I and type II collagen, muscle and type I collagen, and also to determine the orientation of molecules in collagen-based tissues [23,24,34].Therefore, χ^2 seems to be sensitive for detecting structural changes at the molecular scale.

P-SHG has been used previously in two reports for breast cancer detection, however, with mixed results [35,36]. In one study, the researchers used χ^2 to estimate the orientation of collagen molecules in normal and cancerous tissues. Unfortunately, to their surprise, they did not observe any statistical differences between the two [35]. In the same year, another group reported the value of a particular matrix element in χ^2, i.e., d_{22} for normal and breast cancer tissues. d_{22} was normalized with respect to a nonlinear crystal (lithium niobate) and they found significant differences between the two [36]. Here, we sought to examine the potential of SHG imaging for analysis of breast tissue by building on these studies in several significant ways. As a prelude to eventual biomedical research and clinical translation, an overarching consideration in our study is the compatibility with current tissue examination protocols. While the developed methods are sought to be generally applicable to cancer research, we consider the aforementioned four breast tissue conditions as a relevant test case. Furthermore, we also assume a more general crystal class symmetry for collagen, i.e., trigonal symmetry (*3m*), and calculate all the (normalized) tensor elements for the various conditions. Finally, we also determine the unique combination of normalized tensor elements that are most sensitive for characterizing the four tissue conditions. This paper is organized as follows: we first discuss the methodologies of FT-SHG (section 2.1) and P-SHG (section 2.2). Section 3 describes the sample preparation and experimental setup of the SHG microscope. In section 4, we discuss the results and discussion from the two techniques followed by the conclusion in section 5.

2. Methodology

2.1. FT-SHG

Fourier transform-second harmonic generation imaging (FT-SHG) utilizes spatial Fourier analysis on SHG images and can be used to quantify collagen fiber (spatial) organization in biological tissues [26–29]. In this work, the relative, preferred, collagen fiber orientation is considered as a parameter for quantification. To calculate orientation, we employ a custom interactive graphical user interface program in Matlab (MathWorks). Specifically, in our approach, the 2D Fourier transform of a region of interest in an image is calculated, and an angular power spectrum (strength of the various orientations within a particular region) is obtained. This plot is then fitted with a Gaussian distribution, the center of which gives the

#168709 - $15.00 USD Received 21 May 2012; revised 19 Jul 2012; accepted 4 Aug 2012; published 7 Aug 2012

preferred orientation of fibers (multiple fits for several orientations) with respect to a horizontal axis (chosen to be the long axis of the rectangular glass slide used), while the width of the distribution provides a measure of the randomness in fiber orientation. Further, we divide the image into smaller "sub-images", and determine the local fiber orientation within each of these smaller regions.

We define the parameter A.I. ratio as the number of anisotropic to isotropic regions. Regions with fibers having a preferential orientation are categorized as anisotropic, while those with fibers aligned along several different orientations (with no preferred orientation) are considered isotropic. To decide whether a region is isotropic or anisotropic, we look at the angular power spectrum. For example, a single sharp peak in the angular power spectrum corresponds to a region containing fibers that are all oriented along the same direction, while multiple peaks in the power spectrum correspond to several unique directions that fibers are oriented along. Thus, A.I. ratio gives a measure of the number of regions with highly aligned fibers in comparison to those having randomly oriented fibers. Additional details on the methodology behind FT-SHG can be found in Refs. [26–29].

2.2. P-SHG

In general, the induced polarization density (P) in a material is given by

$$P = \chi^{(1)}E + \chi^{(2)}E^2 + \chi^{(3)}E^3 + \ldots, \tag{1}$$

where E is the incident electric field and $\chi^{(n)}$ is the n^{th}-order nonlinear susceptibility. Since SHG is a second-order process, we consider only the second term. Thus, for an incident field with an angular frequency ω interacting with a non-centrosymmetric material, the induced second-order polarization density P at frequency 2ω, can be written as [37,38]

$$P_i(2\omega) = 2\sum_{jk} d_{ijk}E_j(\omega)E_k(\omega), \quad i,j,k = 1,2,3, \tag{2}$$

where d_{ijk} is a 2nd-rank tensor corresponding to the 2nd-order nonlinear susceptibility, and $E_j(\omega)$, $E_k(\omega)$, and $P_i(2\omega)$ correspond to the components of the electric field and polarization density along the three principal axes of the material, respectively. Fortunately, assuming symmetry conditions such as intrinsic permutation, and the fact that P is Hermitian, the d tensor, can be represented as a 3x6 matrix, and therefore Eq. (2) can now be written as [38]

$$\begin{bmatrix} P_x(2\omega) \\ P_y(2\omega) \\ P_z(2\omega) \end{bmatrix} = 2\begin{bmatrix} d_{11} & d_{12} & d_{13} & d_{14} & d_{15} & d_{16} \\ d_{21} & d_{22} & d_{23} & d_{24} & d_{25} & d_{26} \\ d_{31} & d_{32} & d_{33} & d_{34} & d_{35} & d_{36} \end{bmatrix}\begin{bmatrix} E_x(\omega)^2 \\ E_y(\omega)^2 \\ E_z(\omega)^2 \\ 2E_z(\omega)E_y(\omega) \\ 2E_x(\omega)E_z(\omega) \\ 2E_y(\omega)E_x(\omega) \end{bmatrix}. \tag{3}$$

As previously mentioned, we assume collagen fibers to possess the more general crystal class trigonal symmetry ($3m$) [39]. Hence, the d matrix is given by [38]

$$\begin{bmatrix} 0 & 0 & 0 & 0 & d_{15} & -d_{22} \\ -d_{22} & d_{22} & 0 & d_{15} & 0 & 0 \\ d_{31} & d_{31} & d_{33} & 0 & 0 & 0 \end{bmatrix}, \tag{4}$$

where d_{15}, d_{22}, d_{31}, and d_{33} are the only non-zero elements. Therefore, the components of the polarization density are given as

#168709 - $15.00 USD Received 21 May 2012; revised 19 Jul 2012; accepted 4 Aug 2012; published 7 Aug 2012

$$P_x(2\omega) = 2d_{15}E_x(\omega)E_z(\omega) - 2d_{22}E_y(\omega)E_x(\omega)$$
$$P_y(2\omega) = d_{22}\left(-E_x^{\,2}(\omega) + E_y^{\,2}(\omega)\right) + 2d_{15}E_z(\omega)E_y(\omega) \qquad (5)$$
$$P_z(2\omega) = d_{31}\left(E_x^{\,2}(\omega) + E_y^{\,2}(\omega)\right) + d_{33}E_z^{\,2}(\omega) \ .$$

Figure 1 depicts the geometry that we consider for a single collagen fiber relative to an applied optical field. A collagen fiber is oriented along the z-axis while electric field E is incident normal to the y-z plane (along the x-axis), and α is the angle between the incident polarization and the z-axis such that $E_y(\omega) = E \sin\alpha$, and $E_z(\omega) = E\cos\alpha$. Under relatively weak focusing conditions the contribution of the longitudinal field component is much less than that of the transverse components and $E_x(\omega)$ is ~0. We obtain the emitted SHG intensity by taking the sum of the squares of the components of P, and thus obtain

$$I(2\omega) \sim \left[\left(d_{22}\sin^2\alpha + d_{15}\sin 2\alpha\right)^2 + \left(d_{31}\sin^2\alpha + d_{33}\cos^2\alpha\right)^2\right] . \qquad (6)$$

From this equation we observe that the values of the tensor coefficients can be determined to within a constant by fitting the experimental plot of SHG intensity as a function of input polarization (polarization spectrum). Figure 2(a) shows three typical normalized plots of the polarization spectrum that can be obtained from Eq. (6) assuming appropriate values of tensor elements, i.e., d_{15} = 1.0, d_{33} = 1.6, d_{31} = 0.8, and d_{22} = 0.21. Panels (i) and (ii) in Fig. 2(a) shows polarization spectra for nonzero values of d_{22} (–0.21 for (i) and 0.21 for (ii)), which exhibit noticeable asymmetry about 90°. Larger positive values of d_{22} produces the pattern in (i), while larger negative values produces that shown in (ii); values of d_{22} close to zero yield the typical spectral shape shown in (iii). Note that if collagen fiber is assumed to possess cylindrical crystal class (*C6*) symmetry, which is typically assumed, we obtain the spectrum shown in Fig. 2(b), which is the same as that of panel (iii) in 2a. It is clear then that class *3m* is a more general symmetry class of which cylindrical symmetry is a special case.

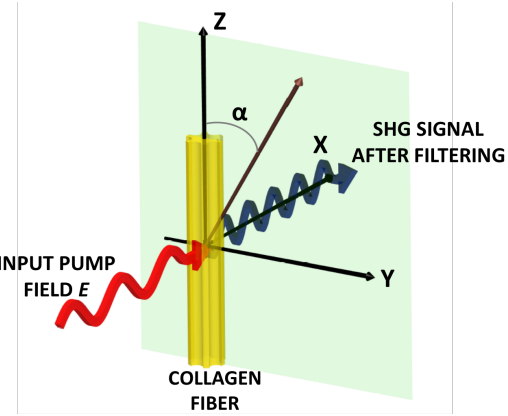

Fig. 1. Illustration of the geometric arrangement of a single collagen fiber relative to an applied electric field. The emitted SHG signal after spectral filtering is shown in blue. Details are provided in the text.

3. Experiment

3.1. Sample preparation

To develop any imaging modality relevant to cancer, a large sampling diversity and number must be incorporated to avoid statistical pitfalls [40]. Tissue microarrays (TMAs) consist of representative tissue materials from a large number of patients that is arranged in a grid format and represent a convenient platform for developing imaging modalities for diagnostic purposes [41,42]. A breast tissue microarray (US Biomax BR1003) was obtained from

#168709 - $15.00 USD Received 21 May 2012; revised 19 Jul 2012; accepted 4 Aug 2012; published 7 Aug 2012

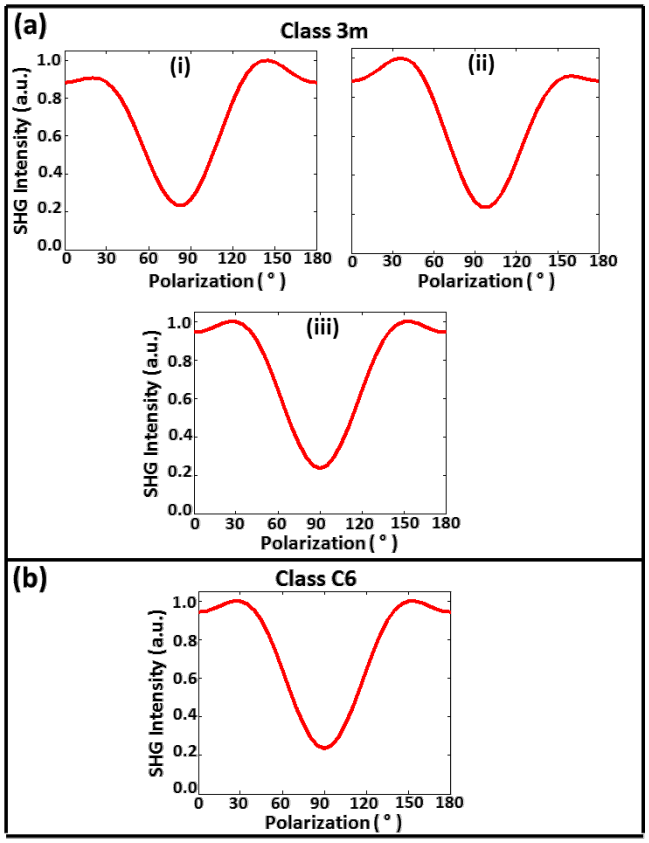

Fig. 2. Simulated plots of normalized SHG intensity as a function of polarization angle (polarization spectrum) for collagen fibers possessing a) trigonal *3m* and b) cylindrical *C6* crystal class symmetry.

formalin-fixed, paraffin-embedded tissue and contained 1-mm diameter circular cores of tissues for different histologic classes — normal, hyperplastic, dysplastic, and malignant (both ductal and lobular carcinoma). These samples were H&E stained and mounted in xylene based mounting medium. The sample thickness is ~5 µm, which is thin enough to produce high-resolution forward SHG images. It is notable that, unlike vibrational spectroscopic imaging techniques that need the sample to be unstained, the sample preparation protocol is entirely compatible with clinical processing.

3.2. Experimental setup

The schematic of the experimental setup for SHG imaging is shown in Fig. 3. An IX81 Olympus microscope is modified to incorporate both backward and forward collection geometries. The light source is a tunable Ti:sapphire laser (Spectra-Physics Mai-Tai HP DeepSee) that produces 100 femtosecond-duration pulses at 80-MHz repetition rate. The beam is linearly polarized and spectrally centered at 800 nm. It is then spatially filtered and collimated before it is scanned by a pair of galvo-mirrors (Cambridge Technology). The polarization incident on the sample is controlled by a polarizer and half-wave plate. The beam is then directed through a combination of relay lenses (scan and tube lens), reflected by a custom-made gold mirror (Lattice Electro Optics Au-B-1”x1”x1mmT) to preserve the polarization state. The polarization ratio at the sample plane is > 600:1. The beam is subsequently focused onto the sample using a 0.6 NA long working distance air objective (Olympus 40X LUCPLFLN) resulting in a focal spot size of ~500 nm. The transmitted signal

#168709 - $15.00 USD Received 21 May 2012; revised 19 Jul 2012; accepted 4 Aug 2012; published 7 Aug 2012

from the sample is collected by a 0.66 NA air objective (Reichert 40X Plan Achromat). The SHG signal is filtered through a laser blocking filter (Semrock FF01-680/SP-25) and a 390/20 nm bandpass filter (Semrock FF01-390/18-25), and collected by an EMCCD camera (Hamamatsu C9100-13). An average power of < 10 mW is used for all experiments.

For P-SHG measurements, the forward-scattered SHG intensity is recorded as the incident polarization is varied between 0° to 180°. We find it sufficient to choose a step size of 30° to produce accurate measures of the *d* ratios. We chose to analyze 11 cores of normal, 10 cores of hyperplastic, 10 cores of dysplastic, and 11 cores of malignant tissue. From each core, regions (~5 µm x 5 µm) containing a collagen fiber were randomly selected for analysis from one of five sectors (top, left, bottom, right, and center). Note that we take discrete measurements within a core as opposed to imaging the core pixel-by-pixel. In total, the respective sample size for normal, hyperplastic, dysplastic, and malignant tissue are 48, 48, 42, and 46. All images are acquired from the surface of the sample to avoid birefringence and diattenuation (at large depths) [43,44], which may further complicate the P-SHG analysis.

In the case of the FT-SHG imaging, the half-wave plate is replaced by a quarter-wave plate to generate circularly polarized light in order to ensure SHG emission from collagen fibers at all orientations. The gold mirror is replaced by a short-pass 760-nm dichroic beam splitter. Tiled backward SHG images are collected to image the whole area (~1-mm diameter) of the tissue core. The same set of filters and detector used in forward geometry are utilized for the backward geometry. For FT-SHG analysis, the number of cores considered for normal, hyperplastic, dysplastic, and malignant tissue are 19, 16, 18, and 29, respectively.

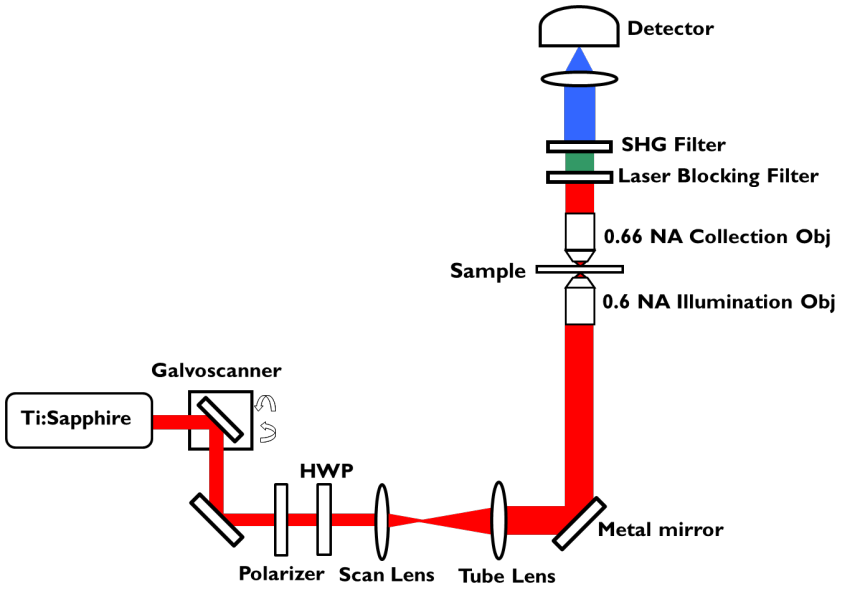

Fig. 3. Experimental setup of the SHG microscope with forward and backward collection geometries. Details of the setup are provided in the text.

4. Results and discussion

4.1. FT-SHG analysis

A diversity of tissue samples, with different pathologic conditions and from different patients, is available using the TMA. Figure 4 shows a selection of tissues in which the brightfield (H&E stained) and SHG images of three representative cores from the four major histologic classes can be compared. The H&E stained images are the gold standard for clinical examination of biopsies. Typically, a manual examination of the H&E images by a pathologist allows for the visualization and identification of the major cell types and locations

#168709 - $15.00 USD Received 21 May 2012; revised 19 Jul 2012; accepted 4 Aug 2012; published 7 Aug 2012

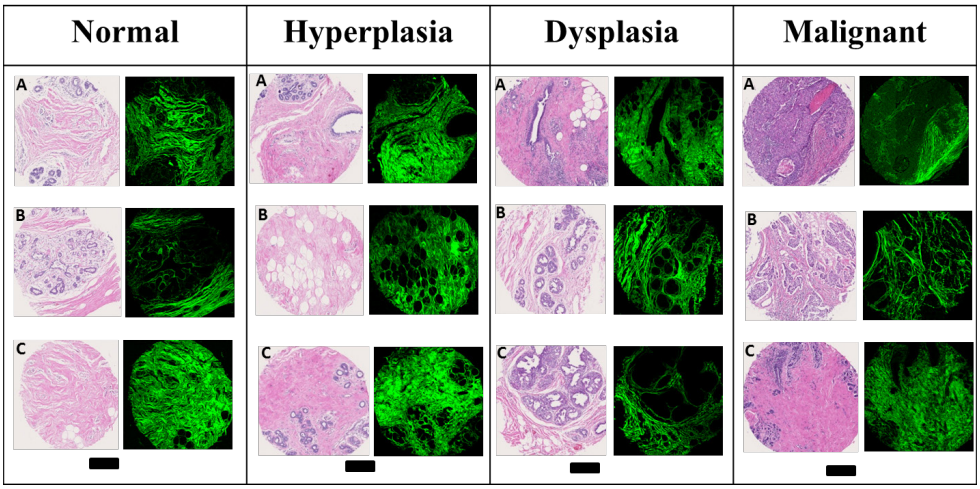

Fig. 4. H&E stained and SHG images of three cores for normal, hyperplastic, dysplastic, and malignant breast tissues. Scale bar: 250 μm.

for imaging. While the H&E stained images provide a comprehensive view of tissue structure, the dye provides a visualization that is fairly non-specific in terms of histologic structures or underlying molecular content. The images shown in Fig. 4 are selected to cover the diversity of the samples and are, thus, generally representative of the histology in breast tissue. The corresponding SHG images are shown alongside the H&E images in which the green color provides a measurable signal and black areas indicate regions without measurable signal. The SHG intensity images provide a complementary, molecularly-sensitive visualization of breast tissue. As is expected, the SHG images are not sensitive to epithelial cells and these are clearly seen as missing from the images. Signal from the stromal regions, however, is large and images are of good quality. The correspondence of tissue histology and complementary information between the H&E and SHG images is enabled by the clinically-compatible protocol developed here. While the combined information can be examined for synergistic effects, we focused here on the information content of SHG images first.

In SHG images, both gross areas of ECM abundance as well as finer structural detail can be observed. As a first level of stromal involvement in tumors, one expects to observe less ECM in larger tumors as the tissue volume is occupied by epithelial cells. That is, of course, a trivial outcome of the histology of solid tumors and not likely to be a very specific diagnostic parameter – hence, we do not focus on that aspect here. We have deliberately chosen TMA sections that contain some ECM for all histologic subtypes in order to analyze the stromal content with SHG. The selection of tissue regions for a valid comparison is not easy as the spatial distribution of cells within the field of view and cellularity within the ECM are obviously different for different pathologic states. Hence, we first wanted to ensure that the samples used in analysis here actually provide a measure of collagen structure and are not influenced by other microstructural entities in the tissues. We examined cellularity in the ECM in terms of the numbers of "dark" regions within the sample. A region is considered dark if the measured SHG intensity is low or negligible, which in the case of breast tissue represents an absence of collagen fibers. Figure 5 shows the bar plot of the number of dark regions within each tissue condition. The calculated values of number of dark regions are 43.6 ± 37.4, 46.6 ± 27.0, 83.2 ± 51.7, and 75.9 ± 61.4 for normal, hyperplastic, dysplastic, and malignant tissue, respectively. Applying a Kolmogorov-Smirnov comparison test, we find that this parameter does not provide any statistically significant differences at the 0.05 level. Hence, our regions used for comparison are truly similar and the underlying morphology will not present a confounding variable.

#168709 - $15.00 USD Received 21 May 2012; revised 19 Jul 2012; accepted 4 Aug 2012; published 7 Aug 2012

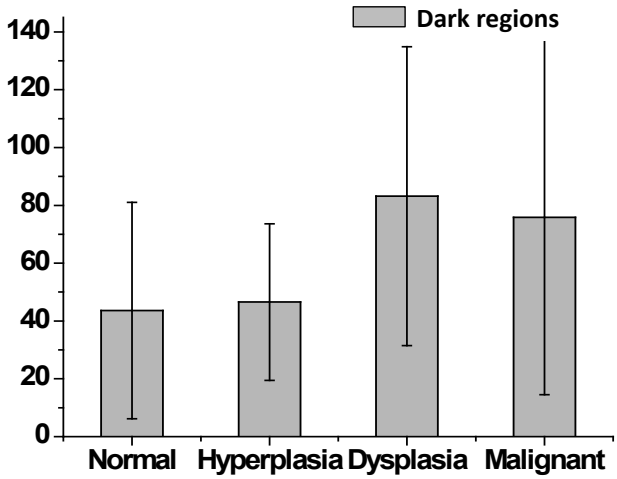

Fig. 5. Bar plot of the number of dark regions for the four tissue conditions.

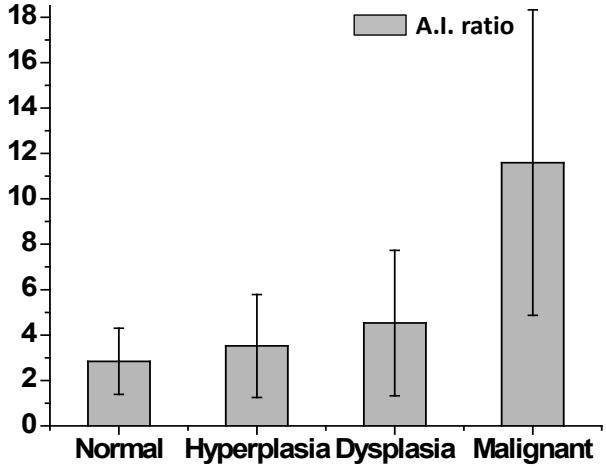

Fig. 6. Bar plot of the parameter, A.I. ratio, for the four pathologic conditions.

Qualitative differences were observed in the stroma between different pathologies but a more quantitative metric is needed for an objective test. Hence, we considered using FT-SHG to determine A.I. ratio for the four pathologic conditions as shown in Fig. 6. We find the calculated values of the A.I. ratio to be 2.8 ± 1.5, 3.5 ± 2.3, 4.5 ± 3.2, and 11.6 ± 6.7 for normal, hyperplastic, dysplastic, and malignant tissue, respectively. It is also observed that the A.I. ratio is the highest for malignant tissue indicating an increased regularity in fiber orientation compared to other tissue conditions. Indeed, Kolmogorov-Smirnov comparison tests showed statistically significant differences in this parameter between the malignant tissue and other conditions at the 0.05 level (note that the actual corresponding p-values are very close to zero which is indicative of the strength of correlation of this parameter). There is also significant variability in the results. This natural variation probably partially accounts for the ambiguous conclusions reported in the literature on using SHG to characterize tumors. We should also caution that the tumor associated stroma is likely associated only closely with the tumor itself. The proximity of the stroma to the tumor in a small TMA sample and our careful attention to ensuring that a fair comparison is made by using-well characterized spots likely explains the observed trend in our study. Significant care must be taken in transferring this result to large areas of unknown tissue. We believe that the observed characteristics of

#168709 - $15.00 USD Received 21 May 2012; revised 19 Jul 2012; accepted 4 Aug 2012; published 7 Aug 2012

malignant tissue arise from a local stiffening of fibroblasts and the attendant stromal remodeling. The spatial extent of this remodeling and its evolution with tumor progression should be studied in detail. Here, our goal was simply to develop a tool that can potentially examine these effects. Hence, we did not pursue a detailed study of stromal remodeling indicative of tumor progression.

4.2. P-SHG analysis

While the previous analysis provided an understanding of multiple collagen fibers' organization at the microscopic level, we also sought to investigate average changes in individual collagen fibers that influence their microscopic organization. Here, we apply P-SHG to calculate the normalized tensor elements of the second-order susceptibility matrix corresponding to collagen fibers. Figure 7 shows example polarization spectra for various conditions. On average, it is observed that collagen fibers in normal tissue (Fig. 7(a)) show prominent shoulders at ~30° and 150° and is relatively symmetric about 90°. In contrast, many fibers in malignant tissue exhibit a polarization spectrum with little or no shoulders and an asymmetry about 90° (Fig. 7(d)). Collagen fibers in hyperplastic and dysplastic tissues show trends that lie between normal and malignant tissues. These trends are likely a consequence of both the remodeling of collagen as well as physical forces in tissue.

Note that Eq. (6) is a proportional equation and as such we can only obtain normalized values of the tensor coefficients. For example, when normalized by d_{15}, we can obtain d_{22}/d_{15}, d_{31}/d_{15} and d_{33}/d_{15}. Note that, however, the choice of normalization is not arbitrary. We want to find the appropriate combination of ratios of tensor elements that contain the least amount of redundancy. For example, if d_{15} is changing with each tissue condition, then other elements normalized by it (d_{22}/d_{15}, d_{31}/d_{15} and d_{33}/d_{15}) will all show the same change, thereby leading to redundancy. To minimize this, we consider all combinations of normalization (i.e., d_{15}, d_{31}, d_{33}, and d_{22}), and the resulting equations are fit to the experimental plot of polarization spectrum for all tissue conditions. We find that in the case of breast cancer, both d_{31} and d_{33} provide the least redundancy; therefore, we choose to normalize the tensor elements by d_{31}. The final expression for the SHG intensity as a function of polarization angle is

$$I(2\omega) \sim \left[\left(\frac{d_{22}}{d_{31}} \sin^2\alpha + \frac{d_{15}}{d_{31}} \sin 2\alpha \right)^2 + \left(\sin^2\alpha + \frac{d_{33}}{d_{31}} \cos^2\alpha \right)^2 \right], \qquad (7)$$

where the ratios d_{22}/d_{31}, d_{15}/d_{31} and d_{33}/d_{31} are calculated and used as metrics to differentiate between breast tissue conditions.

After fitting the experimental plots of the polarization spectrum using Eq. (7), the d ratios, d_{15}/d_{31}, d_{33}/d_{31} and d_{22}/d_{31} (absolute value) are calculated and plots are shown in Fig. 8. The average value of the ratio d_{15}/d_{31} ranges from 0.843 for normal to 0.728 for malignant tissue. Moreover, the standard deviation increases from a value of 0.064 for normal to 0.122 for malignant tissue. Similarly, differences are observed for d_{22}/d_{31} with a mean value of 0.052 for normal and 0.116 for malignant tissue. Again, the standard deviation is observed to be higher for abnormal conditions, likely indicating greater heterogeneity. Interestingly, the ratio d_{33}/d_{31} remains relatively constant across all conditions. These ratios can potentially function as metrics of pathology. There is, however, significant variance indicating the response and heterogeneity of stromal remodeling.

In order to test if the d ratios can be used as a metric for differentiating various breast pathologies, we performed statistical comparison tests assuming the values within the core to be dependent and the values across the cores to be independent. Repeated measures ANOVA with between-subject factors was performed using OriginPro 8 and SAS. A condition for this analysis is that the distribution of values of d ratios must be normal. This is satisfied for the ratios d_{15}/d_{31} and d_{22}/d_{31}, but not with d_{33}/d_{31}. However, for this case, we find that the log of d_{33}/d_{31} also shows a normal distribution thereby permitting us to apply the above analysis. The results of the comparison are shown in Table 1. Using d_{15}/d_{31} and a p-value of 0.05, we find

#168709 - $15.00 USD Received 21 May 2012; revised 19 Jul 2012; accepted 4 Aug 2012; published 7 Aug 2012

that there seems to be the potential to differentiate between normal and dysplasia, normal and malignant, hyperplasia and malignant, and dysplasia and malignant. However, differentiation of hyperplasia from either normal or dysplasia could not be established. Interestingly, we did not observe any statistical differences between ductal and lobular carcinoma-associated stroma.

Given the variance and the range in values, at this stage, it does not appear that there is a simple feature in SHG data that characterizes breast pathology. To more accurately estimate the use of SHG imaging data for breast pathology, we sought to devise a test based on similarity to normal tissue. We defined a filter that contains the range of values of d_{15}/d_{31} for normal tissue and we label the collagen fibers whose tensor values fall outside this normal range as "abnormal" collagen fibers. We then tabulated the number of abnormal collagen fibers in each tissue condition. The fraction of abnormal fibers defined in this manner is plotted for each condition in Fig. 9 and were observed to be 0.0% (by definition), 10.4%, 19.1%, and 47.8% for normal, hyperplastic, dysplastic, and malignant tissue, respectively. It is evident that the number of abnormal fibers is distinctly different for different pathologies. It is also interesting to observe that about 52.2% of the collagen fibers in malignant tissue are normal fibers with this definition. This leads to the conclusion that there are few "global" changes in tissue stroma but different regions must be carefully probed. The second important conclusion is that imaging is needed and averaging measurements will likely yield to confusing results. Thus, studies designed to measure changes due to cancer progression will have to carefully segment the spatial variations and understand these in the context of the tumor. While our goal here was to determine whether there is any potential of using SHG

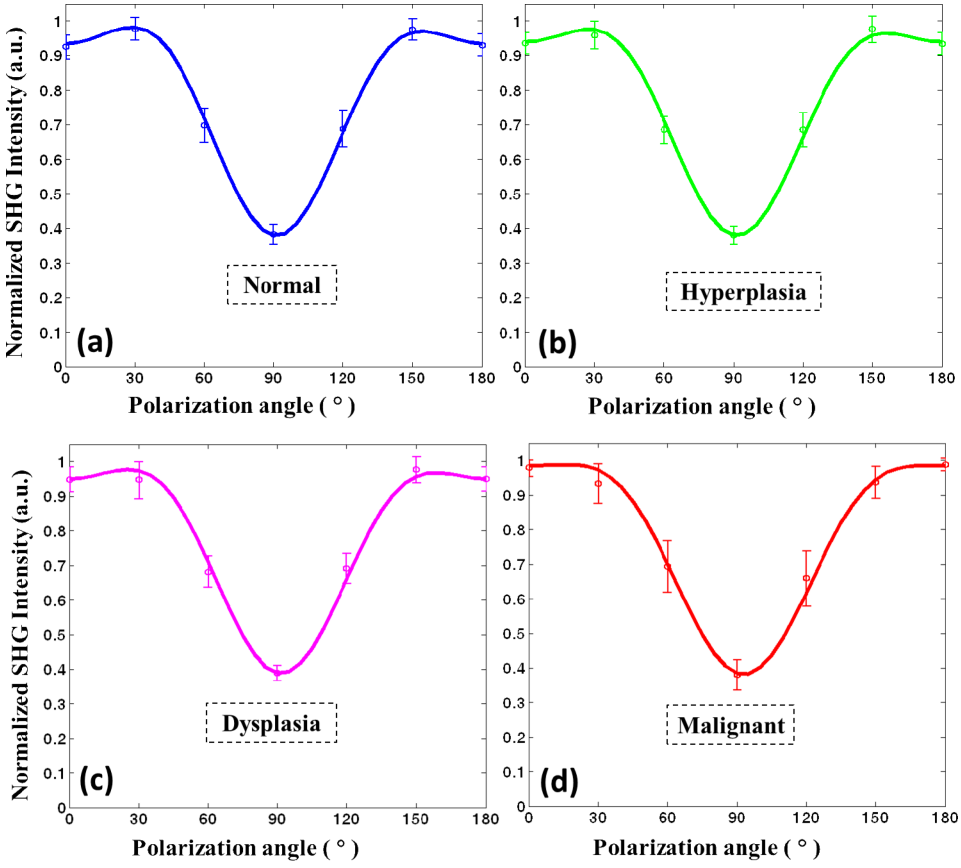

Fig. 7. Normalized SHG intensity as a function of polarization angle (or polarization spectrum) for a) normal, b) hyperplastic, c) dysplastic, and d) malignant breast tissue.

#168709 - $15.00 USD Received 21 May 2012; revised 19 Jul 2012; accepted 4 Aug 2012; published 7 Aug 2012

imaging to understand stromal changes in breast cancer, for future clinical translation, this issue of within sample and other variance must be examined through a larger study and location of fibers relative to the tumor.

As observed from the measurements above, normal breast tissue contains collagen fibers whose d_{15}/d_{31} value lies in the range of 0.843 ± 0.064, and d_{33}/d_{31} within the range 1.570 ± 0.074. These values are close to reported values for type I collagen [24]. The values of d_{22}/d_{31} for normal tissue lie close to zero (0.052 ± 0.043) indicating that the assumption of cylindrical symmetry is valid for normal tissue. This symmetry condition, however, does not seem to

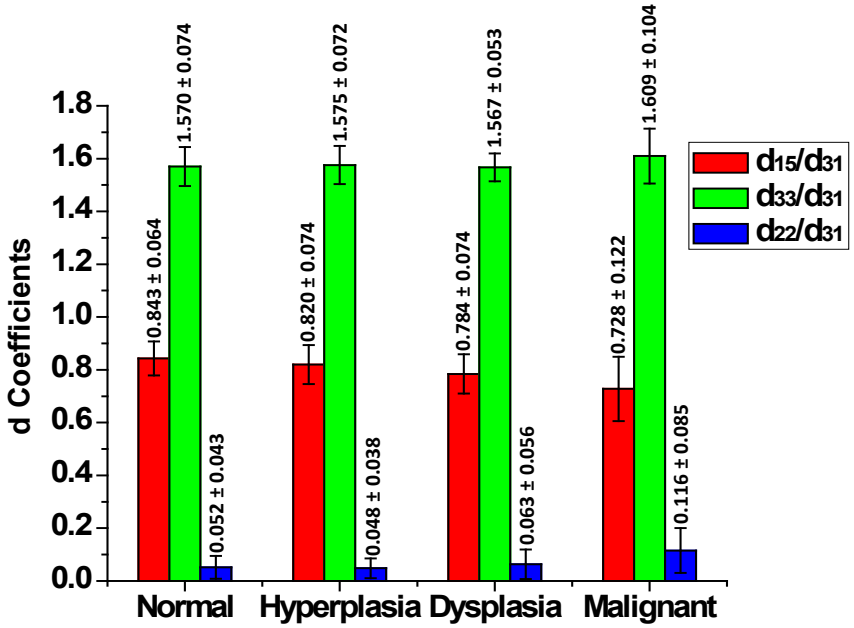

Fig. 8. Bar plot of the tensor elements (d_{15}/d_{31}, d_{33}/d_{31}, d_{22}/d_{31}) for normal, hyperplastic, dysplastic, and malignant tissues.

Table 1. Comparison Tests between Breast Tissue Conditions[a]

	d_{15}/d_{31} (ANOVA)			d_{33}/d_{31} (ANOVA)			d_{22}/d_{31} (K.S. Test)		
Groups	**M.D.**	**p-value**	**S.S.**	**M.D.**	**p-value**	**S.S.**	**M.D.**	**p-value**	**S.S.**
Normal vs. Hyperplasia	0.023	0.3259	No	–0.005	0.8085	No	–0.011	0.9845	No
Normal vs. Dysplasia	0.059	0.0170	Yes	0.003	0.9122	No	–0.012	0.1688	No
Normal vs. Malignant	0.115	<0.0001	Yes	–0.040	0.0438	Yes	–0.064	0.0002	Yes
Hyperplasia vs. Dysplasia	0.036	0.1410	No	0.008	0.7304	No	–0.001	0.1641	No
Hyperplasia vs. Malignant	0.092	0.0003	Yes	–0.034	0.0762	No	–0.053	0.0002	Yes
Dysplasia vs. Malignant	0.056	0.0218	Yes	–0.043	0.0395	Yes	–0.052	0.0135	Yes

[a]The comparison test is performed at a p-value of 0.05, which corresponds to 95% confidence level. M.D. is the mean difference between the different tissue conditions. S.S. is the abbreviation for statistically significant.

#168709 - $15.00 USD Received 21 May 2012; revised 19 Jul 2012; accepted 4 Aug 2012; published 7 Aug 2012

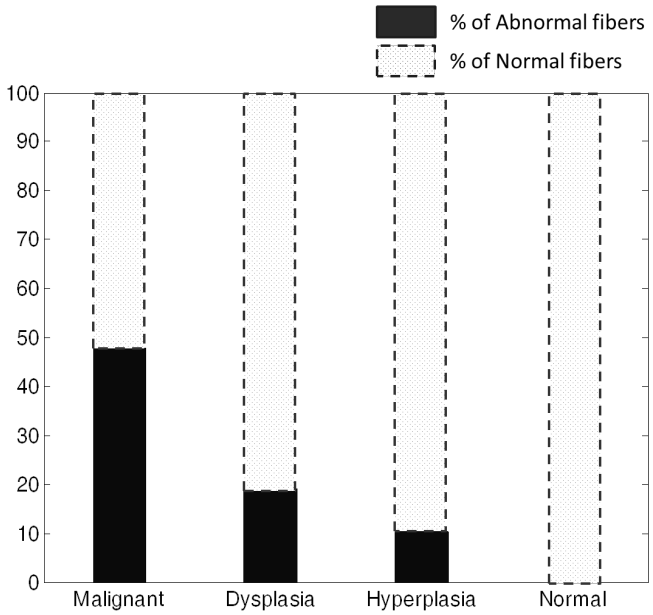

Fig. 9. Percentage of abnormal collagen fibers as a function of breast pathology.

hold for malignant tissues that contain abnormal fibers. Since malignant tissues also contain normal tissue-like fibers (~50% of the total fibers), the average differentiation appears to be smaller. This is also a likely reason for the large standard deviation associated with malignant tissues. Hence, we removed the contribution of normal fibers from malignant tissue and considered only abnormal fibers, which provided values of $d_{15}/d_{31} = 0.646 \pm 0.122$, $d_{33}/d_{31} = 1.603 \pm 0.123$, and $d_{22}/d_{31} = 0.117 \pm 0.087$. Malignant tissue contains fibers that have comparatively smaller d_{15}/d_{31} and larger d_{22}/d_{31} values. Larger values of d_{22}/d_{31} manifest as asymmetry about 90°, and are an indication that trigonal symmetry is a more appropriate description for abnormal fibers. Our observed changes in the values of the d ratios and symmetry are interesting, likely indicating ECM remodeling that is observed during tumor progressions [45]. Molecular changes in collagen fibers were also reported in recent biochemical studies [46,47]: collagen present in the normal tissue is a heterotrimer consisting of two α1(I) chains and one α2(I) chain, while collagen found in malignant tissues are homotrimeric consisting of three α1(I) chains. Unfortunately, resolving these changes are well below the diffraction-limit of conventional optical microscopes but P-SHG allows us to detect potential molecular-level changes optically. Matrix metalloproteinases (MMPs) are also upregulated in cancer [48] and are known to degrade type I collagen fibers. Furthermore, MMP upregulation also leads to a changed isoform of type I collagen, which they do not degrade and helps impart a more aggressive phenotype to cancer cells. Hence, the tools reported in this study can lead to several other basic studies on the mechanism of cancer progression.

5. Conclusion

We utilized two quantitative second-harmonic generation techniques, FT-SHG and P-SHG, to investigate differences in stromal collagen fibers for human breast tissues from different pathologic conditions, namely normal, hyperplasia, dysplasia, and malignant. Using FT-SHG, we quantified collagen fiber organization at cellular scales. We noted the observed differences between various pathologies and developed the metric A.I. ratio as a potentially useful one to differentiate malignant from other tissue conditions. Alternatively, P-SHG was used to infer structural changes in collagen at the molecular scale through the calculation of the normalized tensor elements of the second-order susceptibility. In particular, d_{15}/d_{31} showed statistical

#168709 - $15.00 USD Received 21 May 2012; revised 19 Jul 2012; accepted 4 Aug 2012; published 7 Aug 2012

differences across breast tissue pathologies, except between hyperplasia and normal/dysplasia. We also found that trigonal symmetry (*3m*) is a more appropriate model to describe collagen fibers in malignant tissues as opposed to the conventionally used hexagonal symmetry (*C6*). Furthermore, the percentage of abnormal collagen fibers could potentially be used as a metric for differentiating breast tissue conditions. This unique method of targeting collagen fibers using a combination of two quantitative SHG techniques, FT-SHG and P-SHG, seems promising for further study, especially as a complementary technique with gold-standard histopathological diagnosis. To that end, our SHG measurements were conducted on clinically compatible slides and can be easily incorporated within present clinical work. Future work includes application of quantitative SHG imaging for extension to *in vitro* breast cancer studies as well as other types of cancers.

Acknowledgments

R. A. acknowledges support from the National Science Foundation CAREER award (DBI 09-54155) and R. B. from CHE (0957849). We also thank Hyun-Keun Cho of the UIUC Illinois Statistics office for help with statistics.

#168709 - $15.00 USD Received 21 May 2012; revised 19 Jul 2012; accepted 4 Aug 2012; published 7 Aug 2012